Journal of Metals, Materials and Minerals, 33(4), 1894, 2023

Structural and electrical properties of $0.98(K_{0.5}Na_{0.5}NbO_3)$-$0.02(Bi_{0.5}Na_{0.5}TiO_3)$ ceramics

Swayam Aryam BEHERA[1], Sugato HAJRA[2], Swati PANDA[2], Ali AMANAT[3], and P. G. R. ACHARY[1,*]

[1] *Department of Chemistry, Siksha O Anusandhan University, Bhubaneswar-751030, India*
[2] *Department of Robotics Engineering, Daegu Gyeongbuk Institute of Science and Technology, Daegu-42988, Republic of Korea*
[3] *Department of New Materials and Nanotechnology, National University of Science and Technology MISiS, Moscow, Russia*

***Corresponding author e-mail:** pgrachary@soa.ac.in

Received date:
19 November 2023
Revised date
23 November 2023
Accepted date:
24 November 2023

Keywords:
Lead-Free;
Piezoelectric;
Ferroelectric;
Potassium sodium niobate;
Bismuth sodium titanate

Abstract

In the present communication, lead-free ceramics having composition $0.98(K_{0.5}Na_{0.5}NbO_3)$-$0.02(Bi_{0.5}Na_{0.5}TiO_3)$ were synthesized by a high-temperature solid-state reaction route. The Rietveld refinement for the 0.98KNN-0.02BNT reveals an MPB with phase fraction *Amm2* (87.76 %) and *Pm-3m* (12.27%). The SEM study predicted a mean diameter of 0.98KNN-0.02BNT grains as 0.52 μm ± 0.19. The 0.98KNN-0.02BNTceramic displayed a typical hysteresis loop with a remnant polarization (P_r) of 7.0 $\mu C \cdot cm^{-2}$, saturation polarization (P_s) of 16 $\mu C \cdot cm^{-2}$, and a coercive field (E_c) of 26 $kV \cdot mm^{-1}$. The electrical, Raman spectra, dielectric, and hysteresis loop study supported a morphotropic phase boundary. The synthesized KNN-BNT lead-free material can be an excellent material for designing new devices like ultrasonic transducers and piezo-actuators.

1. Introduction

For numerous reasons, lead-free materials are preferable to lead-based materials. To begin with, lead is very poisonous and presents serious health concerns to both individuals and the environment. Its usage can cause lead poisoning, particularly in children, resulting in developmental disorders and other health consequences. Second, lead-free products are more environmentally friendly and sustainable, decreasing pollution and harm to ecosystems. Furthermore, since international legislation and public awareness discourage the use of lead, lead-free alternatives are becoming increasingly important for compliance and commercial acceptance. Lead-free materials frequently provide equivalent higher performance, making them a safer and more practical alternative in a variety of applications, ranging from electronics to sensors, without sacrificing functionality or safety. Lead-free piezoelectric ceramics are undergoing evaluation for potential applications in ultrasonic transducers [1] and piezo-actuators [2], demonstrating exceptional electroacoustic [3] performance that rivals that of commercial PZT ceramics.

Potassium sodium niobate (KNN) and bismuth sodium titanate (BNT) are two promising lead-free piezoelectric ceramics that have attracted significant attention due to their potential to replace lead zirconate titanate (PZT), a widely used piezoelectric material that contains lead, a toxic heavy metal. These ceramics, KNN ($K_{0.5}Na_{0.5}NbO_3$) and BNT ($Bi_{0.5}Na_{0.5}TiO_3$), have high piezoelectric properties and can be considered to replace lead zirconium titanate [4-7]. Above 690K, KNN stabilizes in cubic-symmetry (*Pm3m)* and tetragonal-symmetry (*P4mm)* within 470 K to 690 K temperature. The tetragonal phase transforms into an orthorhombic phase (*Amm2*) and a rhombohedral phase (*R3m*) when KNN is cooled below 470K and 110K respectively [8]. The structural alteration of BNT with heat becomes complex when compared with KNN. In the study by Jones & Thomas, it was discovered that the material undergoes a phase transformation between 573 K and 593 K, transitioning from the R3c symmetry (low-temperature-ferroelectric-phase) to the P4bm symmetry (high-temperature-phase) [6]. At a temperature of 813 K, a transition known as a morphotropic phase boundary (MPB) occurs, marking the shift from ferroelectric to paraelectric phases, which is a critical point on the phase diagram [9], where the crystal structure quickly changes is where all of them have high piezoelectric characteristics. The KNN system exhibits a diffuse polymorphic phase transition, resulting in a polymorphic phase boundary (PPB) between the orthorhombic and tetragonal phases, extending down to room temperature [10,11]. When the second component is added to a based system, the position of the PPB shifts gradually and continuously to low temperature, forming a gradient line to the composition axis, in contrast to an MPB in a PZT system, which is situated within a limited range of compositions and nearly orthogonal to the composition axis [5,12,13]. While both PPBs and MPBs can induce phase coexistence, PPBs exhibit a greater sensitivity to temperature variations in the crystal structures of nearby compositions. An MPB indicates a change in symmetry as a function of composition, while a PPB represents a change in symmetry as a function of temperature.

The proposed lead-free KNN-BNT ceramic material is expected to exhibit immense potential for innovative device applications such as ultrasonic transducers and piezo-actuators due to its unique MPB composition and favorable electrical characteristics. This novelty

marks a significant stride in the realm of functional materials, paving the way for the development of advanced technologies relying on piezoelectric properties and morphotropic phase boundaries.

In this work, the KNN-BNT was synthesized using a solid-state reaction technique. The material's properties, such as structural, morphological, and electrical properties were evaluated. The lead-free material investigated in this study can be an excellent base for devices such as ultrasonic transducers and piezo-actuators.

2. Synthesis and experimental techniques

Solid state reaction technique was utilized to form the ceramics. At first, the careful ratio of various oxides and carbonate was taken by measurement in a weight balance (M/S Mettler Toledo, USA). Analytical grade of powders of high purity (>99%) was procured from Thermo Fisher, USA, and was poured in an agate mortar pestle. The oxides and carbonates such as K_2CO_3, Na_2CO_3, Nb_2O_5, Bi_2O_3, and TiO_2 were used. The powder was subjected to wet grinding using methanol for 2 h. Then the homogenous mixture was transferred to an alumina crucible and placed inside a furnace. The calcination temperature of the sample was 900°C for 4 h (heating rate 5°C·min^{-1}). Then the powder was grinded finely and blended with PVA as a binder. The powders were then pressed using a pelletizer (4×10^6 N·m^{-2} axial pressure) and disc shape pellets (diameter:12 mm) were obtained. The sintering of the green pellets was carried out by placing them in the furnace at 1100°C for 4 h (heating rate 5°C·min^{-1}). For dielectric and ferroelectric measurements a high-purity silver paste was used to paint it upon both opposite sides of the pellet making it a metal-dielectric-metal arrangement. The required chemical reaction for the synthesis of 0.98KNN-0.02BNT is as follows:

$$0.245(K_2CO_3) + 0.25(Na_2CO_3) + 0.49(Nb_2O_5) + 0.005(Bi_2O_3) + 0.02(TiO_2) \rightarrow [0.98(K_{0.5}Na_{0.5}NbO_3) - 0.02\ (Bi_{0.5}Na_{0.5}TiO_3)] + 0.495(CO_2)$$

A schematic diagram illustrating the synthesis of 0.98KNN-0.02BNT is presented in Figure 1(a).

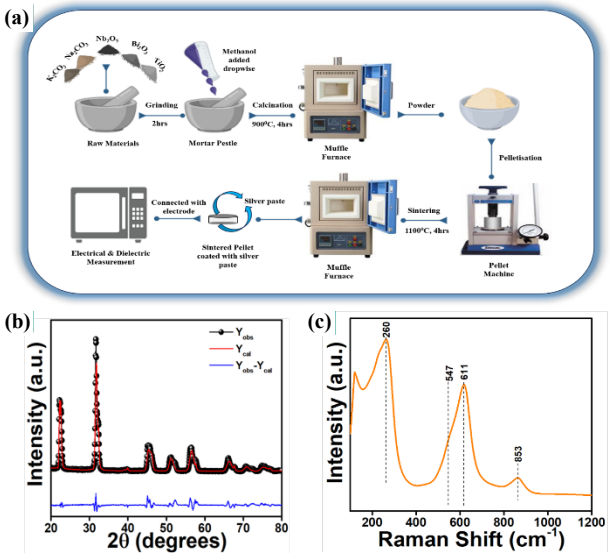

Figure 1. (a) Schematic representation for synthesis, (b) XRD spectra, and (c) Raman spectra of 0.98KNN-0.02BNT

The XRD measurement of ceramic was carried out using a powder X-ray diffractometer (M/S Rigaku Ultima IV, Japan) and the step size was set at 2 degrees/min. Raman spectra were traced using a Raman spectrometer (M/S Thermo Scientific Nicolet, USA) with a 532 nm laser. Polarizations vs. electric field (P–E) hysteresis loops at room temperature were traced by employing Radiant Precision Premier II, USA. The surface morphology of the material was studied by the scanning electron microscope (M/S Hitachi S-4900, Japan). An impedance analyzer (M/S Hioki IM3470) was used to measure the dielectric parameters of ceramics at room temperature and different frequencies. The dielectric parameters include the dielectric constant, the dielectric loss, and the impedance magnitude.

3. Results and discussion

3.1 Structural analysis

Figure 1(b) illustrates the Rietveld-refinement fitting of XRD diffraction patterns of 0.98KNN-0.02BNT, derived using ($10° \leq 2\theta \leq 80°$). An *Amm2+Pm-3m* structural model was employed to analyze the fitting. It is established that the cell parameters of KNN are always described by either orthorhombic) (JCPDS 00-065-0275) or monoclinic (JCPDS 77-0038) [14] unit cells [8,15,16], with a change in the indexes. Considering the width of the 002 peak to be nearly twice that of the 200 peak, a monoclinic symmetry was considered. The emergence of the monoclinic perovskite phase with space group *Pm* signifies the morphotropic phase transition, marking a shift between the orthorhombic phase with space group *Amm2* and the cubic phase with space group *Pm-3m* [17,18]. This transition arises from crystal lattice deformation and distortion induced by BNT substitution. The structural analysis was performed considering the crystal system *Amm2+ Pm-3m*, utilizing lattice parameters that reflect the crystal lattice deformation and distortion. The fitting results yielded slightly better values using *Amm2+Pm-3m*, with Rp = 22.7%, Rwp = 25.8%, and Re = 6.78%. The Rietveld refinement for the 0.98KNN-0.02BNT reveals an MPB with phase fraction *Amm2* (87.76 %) and *Pm-3m* (12.27%) with unit cell volume of 126.77 Å^3 and 60.106 Å^3 perfectly fits.

Raman spectra are applied here to identify local symmetry and understand the movements of molecular frameworks [19]. Six normal vibrations v_i characterize the movements of molecular frameworks (NbO_6) with cubic-O_h-symmetry [20]:

$$\tau_{vib} = A_{1g}(Raman) + E_g(Raman) + 2T_{iu}(IR) + T_{2g}(Raman) + 2T_{2u}(silent)$$

The Raman spectrum of KNN exhibits characteristic peaks corresponding to the internal vibrations of the NbO_6 octahedra. These peaks can be assigned to the following vibrational modes:

v_1: Nb-O bond stretching vibration, with A_{1g} symmetry.
v_2: Doubly degenerate E_g vibrations of O-Nb-O bonds.
v_3: Triply degenerate T_{1u} vibration of Nb-O bonds.
v_4: Triply degenerate T_{1u} vibration of O-Nb-O bonds (bending mode).
v_5: Triply degenerate T_{2g} vibration of O-Nb-O bonds (bending mode).
v_6: Triply degenerate T_{2u} vibration of O-Nb-O bonds (bending mode).

The Raman active normal modes of KNN are $^8A_1$ and $^4A_2$, based on the Pm space group. The KNN-BNT systems were also investigated

by Raman spectroscopy (Figure 1(c)) in the range of 100 cm^{-1} to 1200 cm^{-1} at room temperature. The NbO_6 group in 0.98KNN-0.02BNT shows a symmetric non-degenerated v_1 stretching mode at around 853 cm^{-1}. The v_2 stretching mode is doubly degenerated and splits into two peaks at 611 cm^{-1} and 547 cm^{-1}. The most prominent peak at 260 cm^{-1} corresponds to the triply degenerated v_5 bending mode of the NbO_6 group. The spectra on the side of 0.98KNN-0.02BNT are consistent with these vibrational modes. The different Raman-active modes are in agreement with the literature [21].

Raman spectra for the systems in this communication can be categorized into four distinct regions: (i) Peaks between 100 cm^{-1} to 200 cm^{-1} can be ascribed to Na-O and Bi-O bond vibrations. For example, the peak at 137 cm^{-1} of 0.98KNN-0.02BNT is lined to Na/K-O bond vibrations. This means that there are regions in the material that have a very small size, in the order of nanometers. If these regions were larger, the phonon would not last long enough to produce a clear Raman signal. (ii) The dominance of the Nb/Ti-O vibrational modes (A_1) could be ascribed to the second one around 260 cm^{-1}, (iii) The Raman peaks in the 450 cm^{-1} to 700 cm^{-1} range can be ascribed to the vibration of the NbO_6 or TiO_6 octahedral and (iv) The peaks beyond 700 cm^{-1} could be ascribed to the overlap of A_1&E(LO) bands [21,22]. The presence of different Bi^{3+} and Na^{+} ions causes A-site disorder, which in turn leads to overlapping peaks, resulting in broad peaks.

3.2 Morphological analysis

The morphological study of 0.98KNN-0.02BNT is obtained by scanning electron microscope. The SEM image of 0.98KNN-0.02BNT with particle size distribution is shown in Figure 2(a). There was no particle clumping and all the elements were evenly dispersed. The mean value of the size of 0.98KNN-0.02BNT is 0.52 µm with a standard deviation of 0.19. Energy dispersive spectroscopy (EDS) with elemental percentage composition is shown in Figure 2(b) which was used to trace the mole fraction of each element, indicating that there were no traces of impurities. The elemental color mapping of 0.98KNN-0.02BNT is shown in Figure 2(c), which indicates the existence of elements including Nb, K, O, Na, Bi, and Ti which are all easily distinguishable. EDS spectra confirms that elements At% are as follows: O=60.58, Na=9.23, K=9.19, Ti=0.63, Nb=20.17 and Bi=0.20.

3.3 Polarization-Electric field (PE) loop

The Polarization-Electric field (PE) loop evaluation was carried out at 26°C, 1 Hz, and 4 kV. The 0.98KNN-0.02BNT ceramic displayed a typical hysteresis loop (Figure 3), with a remnant polarization (P_r) of 7.0 µC·cm^{-2}, saturation polarization (P_s) of 16 µC·cm^{-2} and a coercive field (E_c) of 26 kV·mm^{-1}. This is because of the replacement of the predominant order of the ferroelectric (FE) phase by the order of the antiferroelectric (AFE) phase [23,24] and also because of the MPB-phase transformation from rhombohedral/orthorhombic to pseudo-cubic [25].

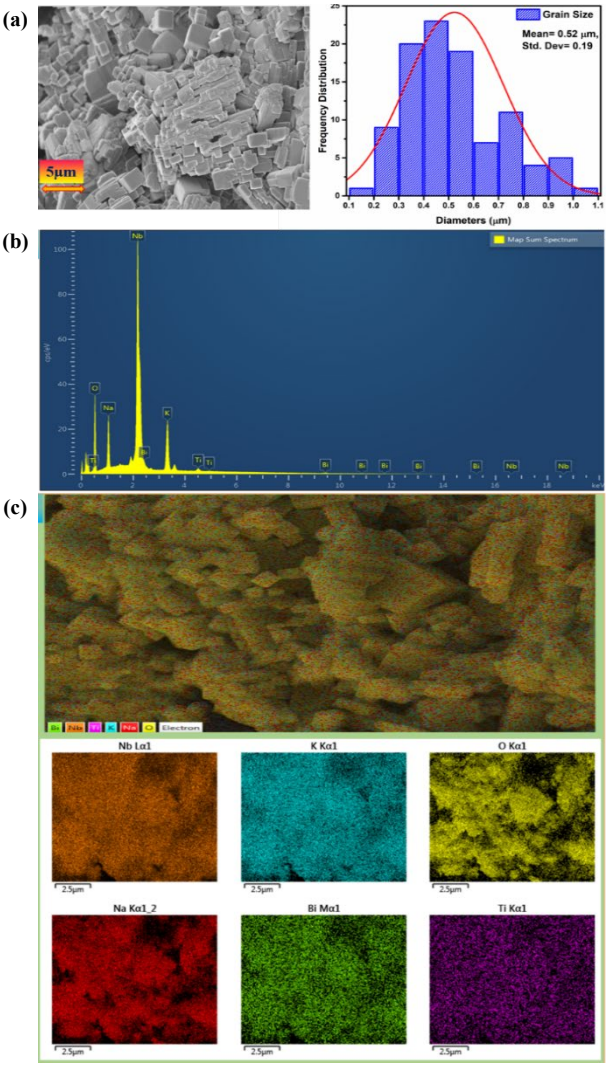

Figure 2. (a) Surface micrograph with size distribution, (b) EDS spectra with elemental percentage composition, and (c) Elemental color mapping of various elements of 0.98KNN-0.02BNT.

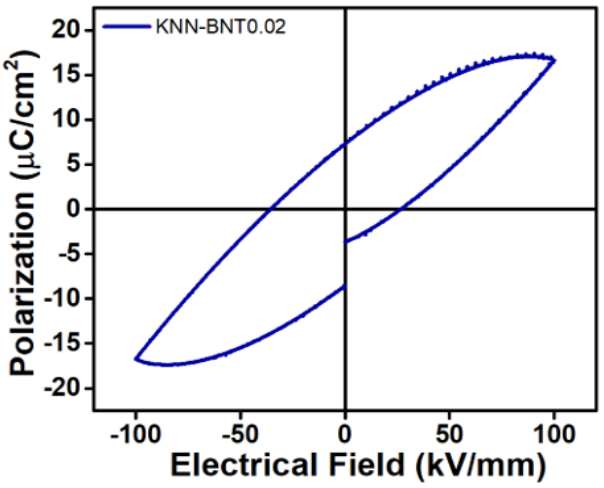

Figure 3. Polarization-Electric field (PE) loop of 0.98KNN-0.02BNT.

3.4 Electrical analysis

The dielectric study of ceramic samples reveals the change in polarization. It is possible to confirm the dielectric constant identified in the transfer function directly by reorienting the dielectric material and neutralizing charge on the electrodes. Assessing the frequency dependence of the dielectric constant is a common method for evaluating the suitability of dielectric materials for device applications. The dielectric constant and dielectric loss characteristics for 0.98KNN-0.02BNT are shown in Figure 4(a) and Figure 4(b) respectively. This would be implied for oxide materials, considering the dielectric characteristics decreased with frequency [26-28]. Several polarization effects, such as interfacial polarization, electronic, and ionic are encountered by the materials at low frequencies. Here, the observed dielectric constant at 100 Hz was 1100.26 and at 100 kHz it was reduced to 830.65, which signifies the above statement. Grain boundaries and grains have important roles at low and high frequencies, respectively [29,30]. In the lower frequency range, the Maxwell-Wagner interfacial polarization[31] and Koop's phenomenology theory [32] may also be useful in explaining the rise in the dielectric constant value. With increasing frequency, polarization effects gradually diminish, leading to a decline in the dielectric constant value. In this region, interfacial polarization plays a more significant role in determining the dielectric constant due to its enhanced contribution at lower frequencies, where electronic polarization dominates. Consequently, as the frequency rises, dielectric loss decreases. This phenomenon is attributed to the lagging of polarization processes (e.g., orientation, space charge, and ions) behind the applied field at higher frequencies. The dielectric loss reduction is a consequence of this behavior [33,34].

Figure 4(c) shows an electrical conductivity (σ_{AC}) plot within the frequency range of 100Hz-100kHz. The frequency has a considerable influence on σ_{AC}. According to the apparent power-law [$\sigma(\omega)= \omega^n$ $(0.6 < n < 1)$], the σ_{AC} values increase with frequency. But here, the σ_{AC} remains constant from the lower to the higher frequency range. A slight increase of σ_{AC} was observed at 100 kHz. The hopping mechanism always satisfies the behavior of the σ_{AC}, where the AC conductivity, in general, rises with the rise in the frequency count [35,36].

Figure 4(d) and Figure 4(e) show the real part of impedance (Z') and imaginary part of impedance (Z'') values (frequency dependent) used to evaluate the resistive properties of 0.98KNN-0.02BNT. Figure 4(f) shows the real vs. imaginary parts of the impedance of 0.98KNN-0.02BNT at room temperature. The impedance of the sample was determined by analyzing the output response resulting from the application of an alternating current signal. Essentially, this approach is particularly effective for analyzing the relaxation process, distinguishing grain boundaries from bulk boundaries, determining the nature of charge carriers, and investigating the polarization effects of materials [37]. The Z' value is considered higher in the low-frequency range and gradually decreases as frequency increases. This lower Z' value represents a rise of σ_{AC} at high frequency. At higher frequencies, the presence of Z' indicates the discharge of space-charges. This factor affects the σ_{AC}, for which the barrier properties are reduced [38,39].

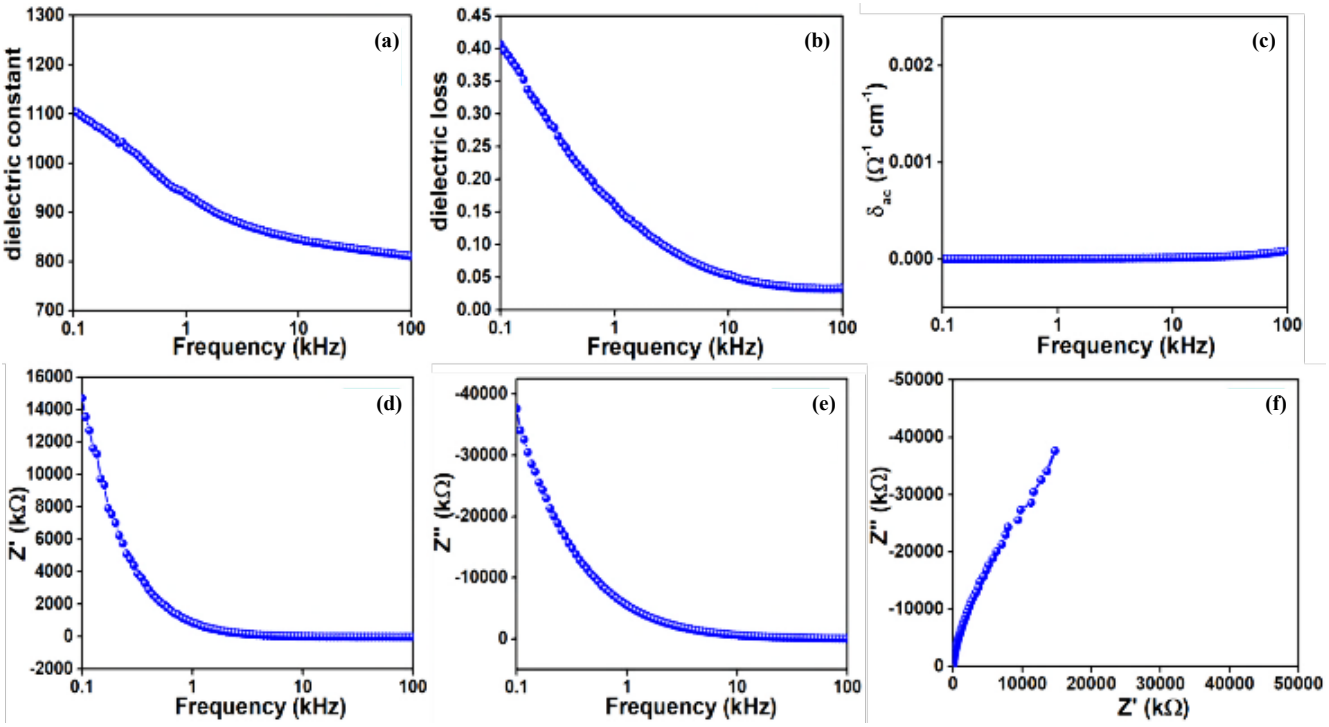

Figure 4. (a) Dielectric constant vs. frequency, (b) Dielectric loss vs. frequency, (c) AC conductivity vs. frequency, (d) Real parts of the impedance vs. frequency, (e) Imaginary parts of the impedance vs. frequency, (f) Real vs. Imaginary parts of the impedance of 0.98KNN-0.02BNT at room temperature.

4. Conclusions

The KNN-BNT (0.98KNN-0.02BNT) was synthesized using a solid-state reaction technique. The material properties, such as structural, morphological, and electrical properties were evaluated. The surface morphology shows the presence of grain and grain boundaries. The elemental colour mapping on the surface of the pellet confirms that there are no impurities present in the sample. The ferroelectric properties of the sample are being investigated. Higher frequencies lead to a reduction in the dielectric constant and dielectric loss. The dielectric constant value of 1100.26 was observed at 100Hz. The impedance spectra are used to evaluate the resistive properties. The lead-free material investigated in this study can be an excellent base for several devices, such as energy harvesters, energy storage or solar cells, ultrasonic transducers, and piezo-actuators.

.

Authors contribution

Swayam Aryam Behera: Formal analysis, Data curation, Writing-Original Draft; Sugato Hajra: Conceptualization, Writing-Original Draft; Swati Panda: Formal Analysis, Ali Amanat: Data Curation, Visualization, PGR Achary: Supervision, Conceptualization, Writing-Editing and Review.

References

[1] M. Bah, F. Giovannelli, F.Schoenstein, C. Brosseau, J-R. Deschamps, F. Dorvaux, L. Haumesser, E. Le Clezio, and I. Monot-Laffez "Ultrasonic transducers based on undoped lead-free (K0.5Na0.5)NbO_3 ceramics," *Ultrasonics*, vol. 63, pp. 23-30, 2015.

[2] K. Wang, F-Z. Yao, W. Jo, D. Gobeljic, V. V. Shvartsman, D. Lupascu, J. Li, and J. Rodel, "Temperature-insensitive (K,Na)NbO_3-based lead-free piezoactuator ceramics," *Advanced Functional Materials*, vol. 23, no. 33, pp. 4079-4086, 2013.

[3] G. C. Edwards, S. H. Choy, H. L. W. Chan, D. A. Scott, and A. Batten, "Lead-free transducer for non-destructive evaluation," *Applied Physics A*, vol. 88, no. 1, pp. 209-215, 2007.

[4] J. Rödel, W. Jo, K. T. P. Seifert, E.-M. Anton, T. Granzow, and D. Damjanovic, "Perspective on the development of lead-free piezoceramics," *Journal of the American Ceramic Society*, vol. 92, no. 6, pp. 1153-1177, 2009.

[5] T. R. Shrout, and S. J. Zhang, "Lead-free piezoelectric ceramics: Alternatives for PZT?," *Journal of Electroceramics*, vol. 19, pp. 113-126, 2007.

[6] T. Takenaka, H. Nagata, and Y. Hiruma, "Current developments and prospective of lead-free piezoelectric ceramics," *The Japanese Journal of Applied Physics (JJAP),* vol. 47, no. 5S, p. 3787, 2008.

[7] P. K. Panda, "Environmental friendly lead-free piezoelectric materials," *Journal of Materials Science*, vol. 44, pp. 5049-5062, 2009.

[8] J. Tellier, B. Malic, B. Dkhil, D. Jenko, J. Cilensek, and M. Kosec, "Crystal structure and phase transitions of sodium potassium niobate perovskites," *Solid State Sciences*, vol. 11, no. 2, pp. 320-324, 2009.

[9] B. Jaffe, W. R. Cook, and H. Jaffe, "The piezoelectric effect in ceramics," *Piezoelectric Ceramics*, pp. 7-21, 1971.

[10] L. Liu, Y. Huang, Y. Li, L. Fang, H. Dammak, H Fan, and M. P. Thi, "Orthorhombic to tetragonal structural phase transition in $Na_{0.5}K_{0.5}NbO_3$-based ceramics," *Materials Letters*, vol. 68, pp. 300-302, 2012.

[11] J. Fu, R. Zuo, and Y. Liu, "X-ray analysis of phase coexistence and electric poling processing in alkaline niobate-based compositions," *Journal of Alloys and Compounds*, vol. 493, no. 1-2, pp. 197-201, 2010.

[12] S. Zhang, R. Xia, and T. R. Shrout, "Modified ($K_{0.5}$ $Na_{0.5}$) Nb O_3 based lead-free piezoelectrics with broad temperature usage range," *Applied Physics Letters*, vol. 91, no. 13, p. 132913, 2007.

[13] Y. Dai, X. Zhang, and G. Zhou, "Phase transitional behavior in $K_{0.5}$ $Na_{0.5}$ Nb O_3-Li Ta O_3 ceramics," *Applied Physics Letters*, vol. 90, no. 26, p. 262903, 2007.

[14] C. Montero-Tavera, M. D. Durruthy-Rodríguez, F. D. Cortés-Vega, and J. M. Yañez-Limón, "Study of the structural, ferroelectric, dielectric, and pyroelectric properties of the $K_{0.5}Na_{0.5}NbO_3$ system doped with Li+, La3+, and Ti4+," *J. Adv. Ceram.*, vol. 9, no. 3, pp. 329-338, Jun. 2020.

[15] K. Singh, V. Lingwal, S. C. Bhatt, N. S. Panwar, and B. S. Semwal, "Dielectric properties of potassium sodium niobate mixed system," *Mater. Res. Bull.*, vol. 36, no. 13-14, pp. 2365-2374, 2001.

[16] S.-Y. Chu, W. Water, Y.-D. Juang, and J.-T. Liaw, "Properties of (Na, K) NbO_3 and (Li, Na, K) NbO_3 ceramic mixed systems," *Ferroelectrics*, vol. 287, no. 1, pp. 23-33, 2003.

[17] H. E. Mgbemere, M. Hinterstein, and G. A. Schneider, "Structural phase transitions and electrical properties of (K_xNa_{1-x}) NbO^{3-} based ceramics modified with Mn," *Journal of the European Ceramic Society*, vol. 32, no. 16, pp. 4341-4352, 2012.

[18] K. Kobayashi, K. Hatano, Y. Mizuno, and C. A. Randall, "Rayleigh behavior in the lead free piezoelectric Lix ($Na_{0.5}K_{0.5}$) 1-xNbO_3 ceramic," *Applied Physics Express*, vol. 5, no. 3, p. 31501, 2012.

[19] J. Swain, A. Priyadarshini, S. Hajra, S. Panda, J. Panda, R. Samantaray, Y. Yamauchi, M. Han, H. J. Kim, and R. Sahu, "Photocatalytic dye degradation by BaTiO3/zeolitic imidazolate framework composite," *Journal of Alloys and Compounds*, vol. 965, p. 171438, 2023.

[20] M. Połomska, B. Hilczer, M. Kosec, and B. Malič, "Raman scattering studies of lead free (1-x)K0.5Na0.5NbO3-xSrTiO3 relaxors," *Ferroelectrics*, vol. 369, no. 1, pp. 149-156, 2008.

[21] L. Liu, M. Knapp, H. Ehrenberg, L. Fang, H. Fan, L. A, Schmitt, H. Fuess, M. Hoelzel, H. Dammak, M. P. Thi, and M. Hintersteing, "Average vs. local structure and composition-property phase diagram of K0.5Na0.5NbO_3-Bi½Na½TiO_3 system," *Journal of the European Ceramic Society*, vol. 37, no. 4, pp. 1387-1399, 2017.

[22] S. P. Biswal, J. Panda, T. Samantaray, J. Swain, N. C. Bera, N. Agasti, V. S. Saji, Dr. R Sahu, R. Samantaray, and J. V. Lockard, "Tuning the optical properties of zirconium-based metal-organic frameworks by post-synthetic modifications," *Materials Letters*, vol. 346, p. 134497, 2023.

[23] A. B. Kounga, S.-T. Zhang, W. Jo, T. Granzow, and J. Rödel, "Morphotropic phase boundary in (1−x)Bi0.5Na0.5TiO_3–

xK0.5Na0.5NbO3 lead-free piezoceramics," *Applied Physics Letters*, vol. 92, no. 22, p. 222902, 2008.

[24] S. Saha, R. P. Singh, A. Rout, A. Mishra, A. Ali, H. Basumatary, and R. Ranjan, "Inducing ferromagnetism and magnetoelectric coupling in the ferroelectric alloy system BiFeO3--PbTiO3 via additives," *Journal of Applied Physics*, vol. 133, no. 6, 2023.

[25] S. Liang, J. Zhu, M. Zheng, P. Zhang, P. Sun, Z. Wang, and X. Zhu, "Microstructure and electrical properties of $(Na_{0.5}K_{0.5})1-2_xMg_xNbO_3$–$Bi_{0.5}Na_{0.5}TiO_3$ lead-free piezoelectric ceramics," *Ceram. International*, vol. 40, no. 2, pp. 2763-2768, 2014.

[26] A. Azam, A. S. Ahmed, M. Chaman, and A. H. Naqvi, "Investigation of electrical properties of Mn doped tin oxide nanoparticles using impedance spectroscopy," *Journal Applied Physics*, vol. 108, no. 9, 2010.

[27] S. A. Behera, R. N. P. Choudhary, and P. G. R. Achary, "Electrical and dielectric properties of EVA/modified lead titanate elastomer composites," *Materials Today: Proceedings*, 2023.

[28] S. A. Behera, S. Panda, S. Hajra, B. K. Panigrahi, H. J. Kim, and P. G. R. Achary, "EVA/PZT composite-based triboelectric nanogenerator for energy harvesting," *Energy Technology, 2023*.

[29] J. Fleig, and J. Maier, "A finite element study on the grain boundary impedance of different microstructures," *Journal of the Electrochemical Society*, vol. 145, no. 6, p. 2081, 1998.

[30] Y.-H. Lin, M. Li, C.-W. Nan, J. Li, J. Wu, and J. He, "Grain and grain boundary effects in high-permittivity dielectric NiO-based ceramics," *Applied Physics Letters*, vol. 89, no. 3, 2006.

[31] T. Prodromakis, and C. Papavassiliou, "Engineering the Maxwell--Wagner polarization effect," *Applied Surface Science*, vol. 255, no. 15, pp. 6989-6994, 2009.

[32] T. M. Meaz, S. M. Attia, and A. M. A. El Ata, "Effect of tetravalent titanium ions substitution on the dielectric properties of Co--Zn ferrites," *Journal of Magnetism and Magnetic Materials*, vol. 257, no. 2-3, pp. 296-305, 2003.

[33] A. Jain, P. KJ, A. K. Sharma, A. Jain, and R. PN, "Dielectric and piezoelectric properties of PVDF/PZT composites: A review," *Polymer Engineering & Science*, vol. 55, no. 7, pp. 1589-1616, 2015.

[34] E. S. Kadir, R. N. Gayen, R. Paul, and S. Biswas, "Interfacial effects on ferroelectric and dielectric properties of GO reinforced free-standing and flexible PVDF/ZnO composite membranes: Bias dependent impedance spectroscopy," *Journal of Alloys and Compounds*, vol. 843, p. 155974, 2020.

[35] D. P. Almond, C. C. Hunter, and A. R. West, "The extraction of ionic conductivities and hopping rates from ac conductivity data," *Journal of Materials Science,* vol. 19, pp. 3236-3248, 1984.

[36] M. Atif, M. Nadeem, R. Grössinger, and R. S. Turtelli, "Studies on the magnetic, magnetostrictive and electrical properties of sol--gel synthesized Zn doped nickel ferrite," *Journal of Alloys and Compounds,* vol. 509, no. 18, pp. 5720-5724, 2011.

[37] J. Fleig, "The grain boundary impedance of random microstructures: numerical simulations and implications for the analysis of experimental data," *Solid State Ionics*, vol. 150, no. 1-2, pp. 181-193, 2002.

[38] A. Yadav, S. Sahoo, S. Singh, I. P. Raevski, and P. M. Sarun, "Influence of Mn-doping on the structure, high-temperature dielectric, and conductive properties of NaNbO3 ceramics," *Materials Science and Engineering: B*, vol. 297, p. 116796, 2023.

[39] S. Mishra and S. K. Parida, "Electrical and optical properties of a lead-free complex double perovskite BaNaFeMoO6: Photovoltaic and thermistor applications," *Materials Science and Engineering: B*, vol. 296, p. 116629, 2023.